Macedonian Journal of Chemistry and Chemical Engineering, Vol. **42**, No. 2, pp. xx–xx (2023)

MJCCA9 –

ISSN 1857-5552
e-ISSN 1857-5625

Received: October 10, 2023
Accepted: November 2, 2023

DOI: 10.20450/mjcce.2023.2776
Original scientific paper

THE ELECTROCHEMICAL REDUCTION OF HYDROGEN PEROXIDE ON A PALLADIUM–AMORPHOUS CARBON COMPOSITE IN AN ALKALINE MEDIUM

Jelena Čović[1*], Valentin Mirčeski[2,3,4], Aleksandra Zarubica[1], Aleksandar Bojić[1], Miloš Marinković[5], Marjan Ranđelović[1]

[1]*University of Niš, Faculty of Sciences and Mathematics, Department of Chemistry, 33 Višegradska St., 18000 Niš, Serbia*
[2]*Faculty of Chemistry, Department of Inorganic and Analytical Chemistry, University of Lódź, Tamka 12, 91–403 Lódź, Poland*
[3]*Institute of Chemistry, Faculty of Natural Sciences and Mathematics, Ss. Cyril and Methodius University in Skopje, Arhimedova 5, 1000 Skopje, N. Macedonia*
[4]*Research Center for Environment and Materials, Macedonian Academy of Sciences and Arts, Bul. Krste Misirkov 2, 1000 Skopje, N. Macedonia*
[5]*Institute of General and Physical Chemistry, Studentski trg 12/V, 11158 Belgrade, Serbia*
covic.jelena91@gmail.com

The study of hydrogen peroxide reduction in an alkaline aqueous medium on a composite of palladium particles dispersed in an amorphous carbon matrix (Pd@AC) was performed. Scanning electron microscopy (SEM), energy-dispersive X-ray spectroscopy (EDX), Fourier-transform infrared spectroscopy (FTIR), and X-ray powder diffraction (XRD) were used to examine morphology, composition, and crystalline structure. The crystalline structure and the size of palladium particles were analyzed using XRD. The reduction of hydrogen peroxide was studied through cyclic and square-wave voltammetry in an alkaline solution in the absence and presence of dissolved oxygen. The overall electrocatalytic effect of Pd@AC toward hydrogen peroxide reduction strongly depends on the presence of oxygen and the hydrogen peroxide disproportionation reaction in a three-phase system of amorphous carbon, palladium particles, and electrolyte solution.

Keywords: hydrogen peroxide reduction; hybrid material; palladium; carbon

ЕЛЕКТРОХЕМИСКА РЕДУКЦИЈА НА ВОДОРОДЕН ПЕРОКСИД НА КОМПОЗИТНА ЕЛЕКТРОДА ИЗГРАДЕНА ОД ПАЛАДИУМ–АМОРФЕН ЈАГЛЕРОД ВО АЛКАЛНА СРЕДИНА

Во овој труд е разработен метод за следење на редукцијата на водород пероксид во алкална средина на композитна електрода изградена од честички на паладиум дисперзирани во аморфен јаглерод (Pd@AC). Скенирачката електронска микроскопија (SEM), енергетско-дисперзивната X-ray спектроскопија (EDX), Fourier-овата трансформативна инфрацрвена спектроскопија (FTIR) и X-ray дифракцијата (XRD) беа користени како техники за студирање на морфологијата, составот и кристалната структура на композитниот материјал. Кристалната структура и големината на честичките од паладиум беа анализирани со техниката XRD. Редукцијата на водороден пероксид беше студирана со примена на циклична волтаметрија и квадратно-бранова волтаметрија во алкален медиум, во присуство и отсуство на кислород. Целокупниот електрокаталитички ефект на композитните честички на Pd@AC во однос на редукцијата на водороден пероксид е функција од присуството на кислород и од реакцијата на диспропорционирање на водороден пероксид во овој трифазен систем составен од аморфен јаглерод, честички од паладиум и електролитен раствор.

Клучни зборови: редукција на водороден пероксид; хибриден материјал; паладиум; јаглерод

1. INTRODUCTION

Hydrogen peroxide (H_2O_2) is a simple molecule that has a significant role in biological systems, waste-water treatment, and bleaching. It is used as an oxidant in chemical synthesis and various fields such as food, clinical, and pharmaceutical industries.[1,2] Many techniques, including titrimetry[3], chromatography[4], spectrophotometry[5], colorimetry[6], chemiluminescence[7], and various electrochemical methods[8–12] have been used for the determination of H_2O_2. However, electrochemical methods are preferred due to their high sensitivity, good selectivity, inexpensive instrumentation, and simple experimental configurations.[10,11] Amperometric, conductometric, and potentiometric electrochemical sensors exhibit various uses in environmental and industrial analyses.[13–16]

Metal nanoparticles have attracted research interest in recent decades due to their electronic, catalytic, and sensory properties.[17–19] Among different materials, noble metal nanoparticles such as Pt, Pd, Cu, Ag, and Au have been used to modify the surface of a working electrode because of their large surface area, long-term stability, and high conductivity.[20] However, noble metals' high cost and scarcity have hindered their promising commercial applications. Moreover, some noble metal-based electrocatalysts are easily poisoned by chemisorbed CO-like intermediates in acid media. Palladium nanoparticles (Pd NPs) are widely studied in electrocatalysis due to their low toxicity, fast electron transfer, and large surface-to-volume ratio.[21] As verified in the literature, Pd is more abundant than Pt. Thus, it can be a good alternative for hydrogen (HRR) and oxygen reduction reactions (ORR) in alkaline media.[22–24] The electrochemical performance of electrodes based on palladium nanoparticles can be improved by using supporting materials. [25] Palladium on a support material results in lower onset potential and higher electrocatalytic activity with reduced loading of the noble metal on the catalyst. This significantly reduces the cost of the catalyst, making it a competitive alternative to unsupported (bulk) catalysts.[22]

Embedding Pd particles in an amorphous carbon matrix during composite processing allows tighter integration of the metal than adding them on top of the support. The tight and compact composite structures achieved markedly enhance the electrochemical properties of amorphous carbon (AC) with intrinsic Pd particle distribution. Hence, catalyst development has been focused on improving kinetic current densities and lowering applicable H_2O_2 onset potential toward more energy-efficient perspective demands.

This study presents the synthesis of a palladium-amorphous carbon composite (Pd@AC) and its characterization using SEM, EDX, XRD, and FTIR. Its electrochemical behavior was evaluated in alkaline aqueous solutions through cyclic voltammetry (CV) and square-wave voltammetry (SWV) in the presence and absence of oxygen in the potential range from +0.2 V to −0.6 V. The study focuses on understanding the mechanism of the hydrogen peroxide reduction reaction (HPRR) influenced by mass transfer, adsorption, and spontaneous H_2O_2 disproportionation at the amorphous carbon/palladium particle/electrolyte solution interface. To our knowledge, this is the first study of H_2O_2 reduction on Pd-alloyed amorphous carbon particles, providing a benchmark for future studies.

2. EXPERIMENTAL SECTION

2.1. *Synthesis of phenol formaldehyde resin*

Phenol (9.41 g) was dissolved in 4 ml of water with 0.8 g NaOH, then 16.4 ml of formaldehyde was added. The obtained solution was heated to 100 ºC for 3.5 hours, then cooled to room temperature and neutralized with conc. H_2SO_4 (1:3 *v*/*v*). The obtained resin was washed several times with deionized water to a neutral pH.

2.2. *Synthesis of palladium amorphous carbon (Pd@AC) composite*

First, 50 mg of $PdCl_2$ was dissolved in 0.05 mL of concentrated HCl and heated at 60 °C for 30 min. The solution was cooled, diluted with deionized water to 4 ml, and then added to 4 ml of an aqueous solution of 25 mg cetyltrimethylammonium bromide (CTAB). At the end, 2 ml of an aqueous $NaBH_4$ solution (10 g/l) was added, and the resulting suspension was centrifuged and washed several times with ethanol. The residue was thoroughly mixed with phenol-formaldehyde resin in an ultrasonic bath for 15 min. After that, the Pd@AC composite was dried at room temperature. The carbonization step was performed in a laboratory tube furnace at 1000 °C for 2 h, under an argon atmosphere, with a heating rate of 2 °C/min. Finally, the material was powdered in an agate mortar and packed in a tightly closed container.

2.3. *Electrode preparation*

A glassy carbon electrode (GCE) was polished on a polishing cloth with a 0.05 μm Al_2O_3 powder slurry and rinsed with deionized water. A mass of 5 mg Pd@AC powder was dispersed in 1 ml of an ethanol/water mixture (40%, *v*/*v*), and the suspension was homogenized in an ultrasonic bath for 30 min. Then, 5 μl of the suspension was transferred onto the surface of the GCE and dried under a N_2 stream. The final step was to cover the already modified electrode surface with 5 μl of 0.05 % (mass percentage) Nafion solution in ethanol and dry it again under the N_2 stream. This modified GCE was used for the electrochemical analysis of H_2O_2. The Nafion thickness was calculated to be around 0.2 mm. The bare GC electrode was examined to study the electro-reduction of H_2O_2 without the Nafion layer. It is worth noting that oxygen and hydrogen peroxide can permeate a thin Nafion membrane (a few mm) and thus can be reduced at the electrode surface.[26,27]

2.4. *Electrochemical analysis*

The electrochemical analysis was performed using a three-electrode system with a potentiostat (PalmSens4) at room temperature. A saturated calomel electrode (SCE) was used as a reference, a graphite bar was used as an auxiliary electrode, and the palladium amorphous carbon (Pd@AC) composite modified glassy carbon (GC) was used as a working electrode. A solution of 5 mM H_2O_2 in 0.1 M KOH was used to examine the electrocatalytic behavior of the Pd@AC composite in air-saturated solutions. The supporting electrolyte was purged with nitrogen gas for thirty minutes for experiments in oxygen-free solutions.

2.5. *Characterization*

The Pd@AC composite was characterized by scanning electron microscopy (SEM), X-ray powder diffraction (XRD), and Fourier transform infrared spectroscopy (FTIR). SEM images were obtained using a JEOL JSM 6610 LV (Japan) scanning electron microscope in conjunction with an EDS detector, model X-Max Large Area Analytical Silicon Drift, connected to an INCAEnergy 350 Microanalysis (detection of elements $Z \geq 5$; detection limit, ~ 0.1 mass. %; resolution 126 eV). The XRD of the sample was measured on an STADI P instrument from STOE & Cie GmbH with a Mythen1K detector. Cu-Kα-radiation was used at 40 kV and 40 mA. FTIR spectroscopy was carried out using an FTIR spectrometer (Bomem MB-100, Hartmann & Braun, Canada).

3. RESULTS AND DISCUSSION

3.1. *Characterization of palladium resin composite*

The morphology of the Pd@AC composite was analyzed using SEM, as shown in Fig. 1a-b. The chemical composition, concentration, and distribution of elements for the Pd@AC composite were determined using energy-dispersive X-ray spectroscopy (EDX). The EDX spectra of the Pd@AC composite with corresponding peaks are presented in Figure 1c.

The EDX analysis indicated that the Pd@AC composite consisted of 86.75 wt.% C, 11.13 wt.% O, and 2.13 wt.% Pd. Figure 1c shows uniform arrays of Pd clusters with sizes controlled by several tens of micrometers and nonuniform interparticle distance.

It can be seen that Pd particles (agglomerates) in the composite structure are very finely dispersed and relatively homogeneously distributed. They can be observed as very small Pd-rich areas inside the amorphous carbon matrix with a mass fraction of 2.1 %. Most of the Pd is likely located inside the matrix and covered by a carbon layer. The composite particles have sharp edges formed by larger pieces breaking during the shredding of the material in an agate mortar to the desired granulation. Additionally, some grains exhibit macroporosity, attributed to the intense release of gases and fumes during the carbonization step.

The crystalline structure and average crystallite size of the Pd@AC composite were defined using XRD and presented in Figure 2.

The intense broad peak at 23.72º shows that the synthesized Pd@AC composite has an amorphous characteristic with certain clearly defined sharp peaks originating from palladium.[28] Several reflections observed in Fig 2 at around 2-theta angles of 40.2º, 46.8º, 68.2º, 81.95º, and 86.63º are ascribed to the (111), (200), (220), (311), and (222) crystal facets of Pd (JCPDS card no. 46-1043).[29]

The lattice parameter (αPd) values of the metal particles were obtained using the Pd (220) diffraction peak of the composite. The lattice constant value of dispersed Pd nanoclusters was calculated to be 3.886 Å using Eq 1. This is slightly lower than the ideal value of 3.890 Å for pure Pd.

$$\sin(\theta) = \frac{\lambda\sqrt{h^2+k^2+l^2}}{2a} \qquad (1)$$

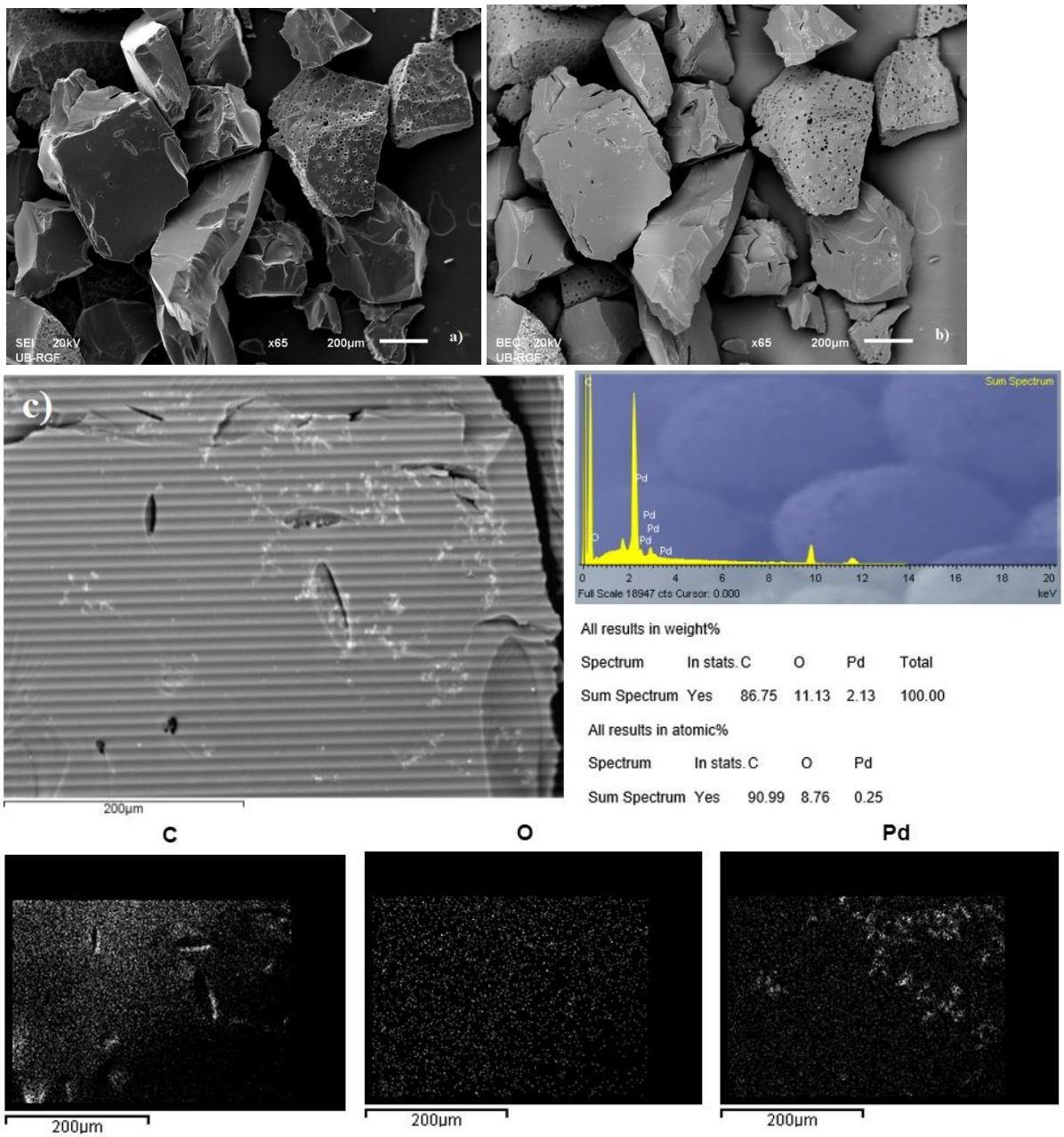

Fig. 1. (a) and (b) SEM microphotographs of Pd@AC composite, (c) EDX spectra of Pd@AC composite

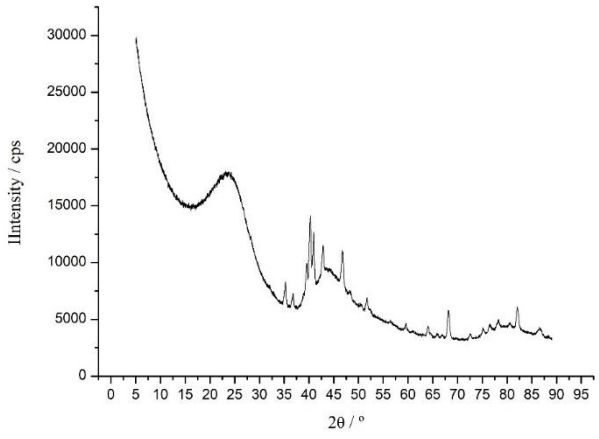

Fig. 2. XRD pattern of Pd@AC composite

Based on the (220) diffraction, the average crystallite size was calculated using Scherrer's equation (Eq. 2), and the value obtained was 15.75 nm.

$$D = \frac{K\lambda}{\beta\cos\theta} \quad (2)$$

where K = 0.89 is Scherrer's constant related to the crystallite shape, λ is the X-ray wavelength (λ = 0.154 nm), the FWHM value of the Pd (220) diffraction peak shown by β, and θ is the diffraction angle.[30] The presence of broad peaks in the pattern indicates that the carbon matrix is amorphous with characteristic broad reflections in the region of 2θ angles around 25°, 45°, and 80° which correspond

to (002), (101), (110) atomic planes, potentially graphite carbon.

The infrared spectrum of a Pd@AC composite in the 400–4000 cm^{-1} range is displayed in Figure 3. According to the literature, there are several characteristic peaks in the absorption bands of the spectrum. The peaks at 3896.65 cm^{-1}, 3763.58 cm^{-1} and 3443.92 cm^{-1} are ascribed to the stretching vibration of the hydroxyl group.[31,32] The peak at 2883.19 cm^{-1} confirms the existence of out-of-phase stretching vibration of -CH_2- alkane, while the peak at 1809.47 cm^{-1} is attributed to the C–C stretching of a benzene ring.[26,33] The peaks related to the C=C aromatic ring and O–H bending vibration of phenols appeared at 1609.86 cm^{-1} and 1423.27 cm^{-1}, respectively.[25,26] The peak at 1110.37 cm^{-1} is assigned to the C–O–C asymmetric stretching vibration.[26] The low-intensity peaks at 880.87 cm^{-1} and 606.05 cm^{-1} belong to the C–H deformation of the out-of-plane substituted ring and the C–H bond of the benzene rings, respectively.[25–27]

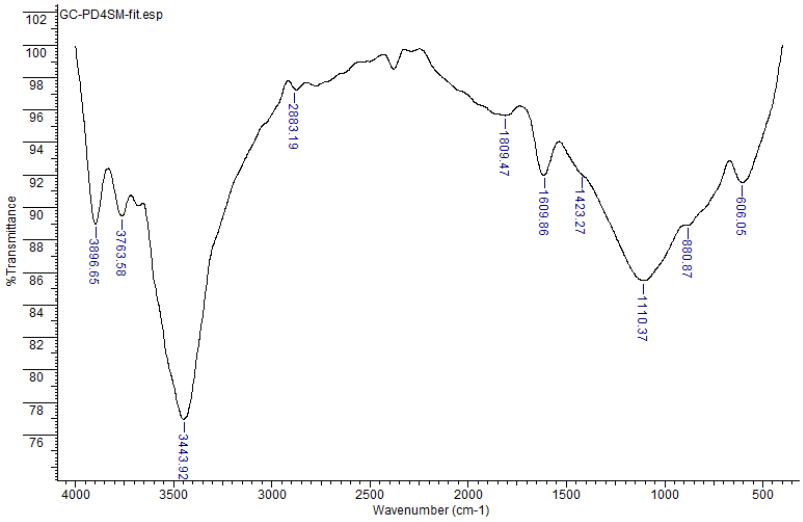

Fig. 3. The FTIR spectrum of Pd@AC composite in the range of 400–4000 cm^{-1}

3.2. *HPRR (hydrogen peroxide reduction reaction)*

To investigate the reduction of hydrogen peroxide at a Pd@AC modified GC electrode, cyclic voltammetry and square-wave voltammetry were performed in degassed and air-saturated 0.1 M KOH solutions. Firstly, one must consider the typical voltammetric characteristics of a palladium electrode in a basic medium, which are strongly influenced by adsorption phenomena and electrocatalytic oxidation of hydroxide ions. These processes form adsorbed oxygen and palladium hydroxides, which undergo subsequent electrocatalytic reduction. In the presence of dissolved oxygen, the electrochemical behavior of the palladium electrode in a basic medium is similar, but the competitive adsorption of oxygen with hydroxide ions leads to some differences.

The presence of hydrogen peroxide adds complexity to the overall electrochemistry. In addition to the previously described processes, hydrogen peroxide can be directly electrocatalytically reduced at the palladium electrode. However, at the same time, its spontaneous disproportionation reaction to water and oxygen occurs in the bulk of the basic solution (Eqs. 3 and 4)[34,35] as well as on the surface of the palladium nanoparticles (Eqs. 5 and 6), as demonstrated in our recent study:[27]

$$H_2O_2(aq) + OH^-(aq) \leftrightarrows HO_2^-(aq) + H_2O(aq) \quad (3)$$

$$2HO_2^-(aq) \leftrightarrows O_2(aq) + 2OH^-(aq) \quad (4)$$

$$2HO_2^-(ads) \leftrightarrows O_2(ads) + 2OH^-(ads) \quad (5)$$

$$O_2 + 2H_2O + 2e^- = HO_2^- + OH^- \quad (6)$$

Figure 4 summarizes typical cyclic voltammetric data to reveal some aspects of the complex electrochemistry resulting from the electrocatalytic effect of the Pd@AC catalyst. The effect of the electrocatalyst in the presence of hydrogen peroxide is apparent from the comparison with the bare GC electrode, as shown in Figure 4A. However, the origin of the voltammetric response in the presence of H_2O_2 is not immediately apparent, given the numerous possible electrochemical and chemical (redox disproportionation) reactions discussed

above. To shed light on this, Figure 4B compares the typical cyclic voltammetric response in the absence of hydrogen peroxide and dissolved oxygen at both the bare and Pd@AC modified GC electrodes. A strong, irreversible electrode process occurs at the Pd@AC electrode in a blank KOH solution, likely due to the electrocatalytic reduction of an adsorbed oxygen species. This species is formed in situ on the electrode surface at potentials more positive than –0.2 V by the electrocatalytic oxidation of adsorbed hydroxide ions.

The voltammetric data shown in Figure 4C support the previous assumption that the typical response with a peak potential close to –0.480 V is mainly due to catalytic oxygen reduction because it is present even in the absence of H_2O_2. Additionally, Figure 4D compares the electrocatalytic effect in the presence of oxygen and hydrogen peroxide, demonstrating that the latter case provides the strongest catalysis due to the complex interplay of oxygen reduction and in situ disproportionation of the hydrogen peroxide at palladium nanoparticles. This follows the reaction scheme developed in our previous study.[27]

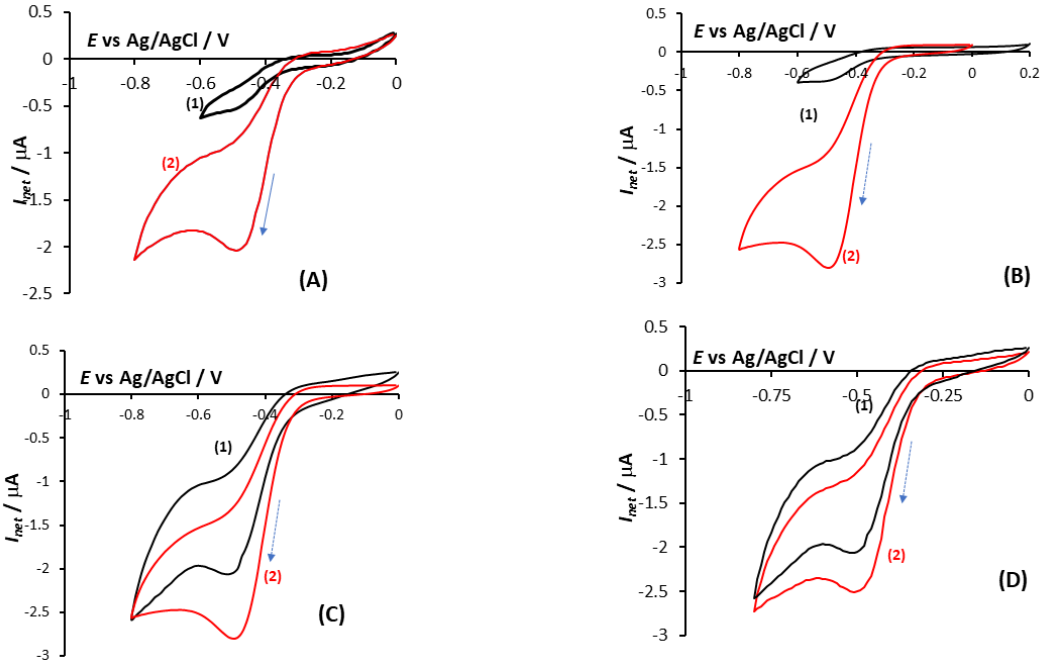

Fig. 4. Typical cyclic voltammograms recorded in 0.1 mol/l KOH supporting electrolyte at the scan rate of 10 mV/s. **(A)** Cyclic voltammograms in 5 mmol/l H_2O_2 in a degassed solution at a bare GC electrode (1) and the Pd@AC modified GC electrode (2). **(B)** Cyclic voltammograms in the absence of H_2O_2 in a degassed solution at a bare GC electrode (1) and at the Pd@AC modified GC electrode (2). **(C)** Cyclic voltammograms at the Pd@AC modified GC electrode in the absence of H_2O_2 and a degassed solution (1) and in a saturated solution (2). **(D)** Cyclic voltammograms at the Pd@AC modified GC electrode in air-saturated solution in the absence of H_2O_2 (1) and in the presence of 5 mmol/l H_2O_2 (2).

The data obtained by Tafel analysis of the rising part of cyclic voltammograms support the electrocatalytic character of the electrode reaction in the presence of the Pd@AC catalyst in degassed solutions. Table 1 compares Tafel data pertinent to a bare GC electrode and the Pd@AC modified electrode, using the following equations:[36,37]

$$\eta = a + b\log(i) \quad (6)$$

$$b = -2.3\frac{RT}{\alpha nF} \quad (7)$$

where η is the overpotential, which represents the difference between the electrode potential and the equilibrium open-circuit potential ($\eta = E - E_{eq}$; for Pd@AC E_{eq} = –126.9 mV, for $c(H_2O_2)$ = 5 mM), a is the intercept ($a = 2.3RT/(\alpha nF)[\log(i_0)]$), b is the Tafel slope, R is the universal gas constant (8.314 J mol^{-1} K^{-1}), T is the temperature (taken as 295.15 K), α is the electron transfer coefficient, n is the stoichiometric number of exchanged electrons, i is the current density, and i_0 is the exchange current density.

T a b l e 1

Tafel analysis of cyclic voltammograms recorded at the scan rate 10 mV/s at a bare GC electrode and the Pd@AC modified GC electrode in a degassed 0.1 M KOH supporting electrolyte in 5 mM H_2O_2

Electrode	E_{on} (mV)	I_0 (μA cm^{-2})	E_{eq} (mV)	$n\alpha$	Tafel slope (mV dec^{-1})	E_p (V)	I_p (μA)
GC	–356	4	–119	0.15	358.4	–0.48	–0.12
Pd@AC	–241.5	147	–126.9	0.50	117.5	–0.48	–1.096

Table 1 shows that the Pd@AC composite exhibited a smaller Tafel slope of 117.5 mV/dec compared to the bare GC electrode (358.4 mV/dec), indicating that the Pd@AC composite has more favorable electrode reduction kinetics. Furthermore, the catalytic activity of the Pd@AC composite was also indicated by the exchange current density (i_0) values and onset potential (E_{on}). In addition, Table 2 presents Tafel data obtained in an air-saturated 0.1 M KOH solution, supporting the electrocatalytic effect of the Pd@AC modified electrode. However, comparing data in Tables 1 and 2, such as the onset potential, slope, and exchange current density, slight differences can be noted, implying that the overall electrode mechanism depends on the presence of oxygen in the solution. Specifically, in an air-saturated solution, the disproportionation reaction (4) in the bulk of the solution is likely to be significantly shifted to the side of reactants, making the bulk hydrogen peroxide disproportionation reaction insignificant. On the other hand, how strongly the surface disproportionation reaction (5) is precluded in the presence of oxygen depends on the relative strength of the competitive adsorption of oxygen, hydroxide ions, and hydrogen peroxide (Eq. 7). In contrast, in the absence of oxygen, both bulk and surface disproportionation reactions occur concomitantly.

T a b l e 2

Tafel analysis of cyclic voltammograms recorded at the scan rate 10 mV/s at a bare GC electrode and the Pd@AC in an air-saturated 0.1 M KOH supporting electrolyte in 5 mM H_2O_2

Electrode	E_{on}(mV)	I_0 (μA/cm^2)	E_{eq} (mV)	na	Tafel slope (mV/dec)	E_p (V)	I_p (μA)
GC	–352	1.64	–250	0.84	69.4	–0.37	–3.3
Pd@AC	–298	115.4	–124.5	0.49	120.05	–0.49	–1.257

The scan rate variation over the interval from 20 mV/s to 100 mV/s at the Pd@AC modified electrode in 0.1 M KOH containing 5 mM H_2O_2 reflects the complexity of the electrode mechanism in accordance with the previous data. Specifically, the cathodic peak current increases non-linearly by increasing the scan rate (Fig. 5), regardless of the presence of oxygen, deviating from the theoretical prediction based on the Randles-Ševčík equation for simple irreversible two-electron electrode reaction of a dissolved redox species.[38] Importantly, at scan rates lower than 20 mV/s, the peak current decreases by increasing the scan rate. A plausible explanation for such a complex influence of the scan rate could be found in a reaction mechanism where the electrode reaction is gated by a preceding chemical reaction, i.e., a CE type of mechanism. Thus, particularly in the absence of oxygen (curve 2 in Fig. 5), the disproportionation of H_2O_2 at the surface of Pd particles proceeds as a heterogeneous process (Eq. 5), as well as spontaneous disproportionation in the bulk of the solution (Eq. 4) to form either adsorbed or dissolved oxygen.

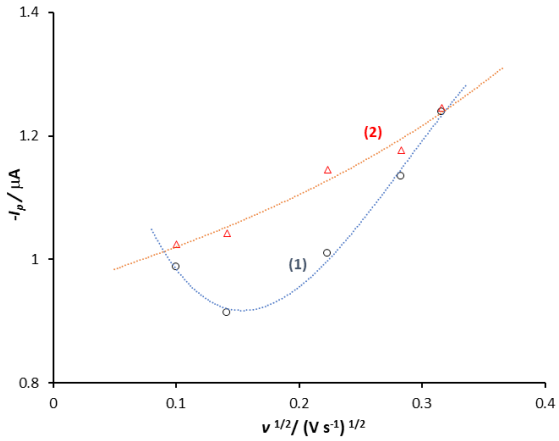

Fig. 5. Variation of the cathodic peak-current of cyclic voltammograms with the square root of the scan rate recorded at the Pd@AC modified GC electrode in 0.1 mol/l KOH supporting electrolyte containing 5 mmol/l H_2O_2 in a degassed solution (1) and in air-saturated solution (2)

Thus, Eqs. 4 and 5, together with the electrode reduction of oxygen reduction, complete a complex $C_{het}E$ type reaction scheme, as theoretically elaborated in our recent study.[39]

Further mechanistic insight has been provided by square-wave voltammetry; the data is summarized in Figure 6. Typical net SW voltammograms presented in Figure 6A support the catalytic effect of the Pd@AC composite compared to the bare GC electrode.

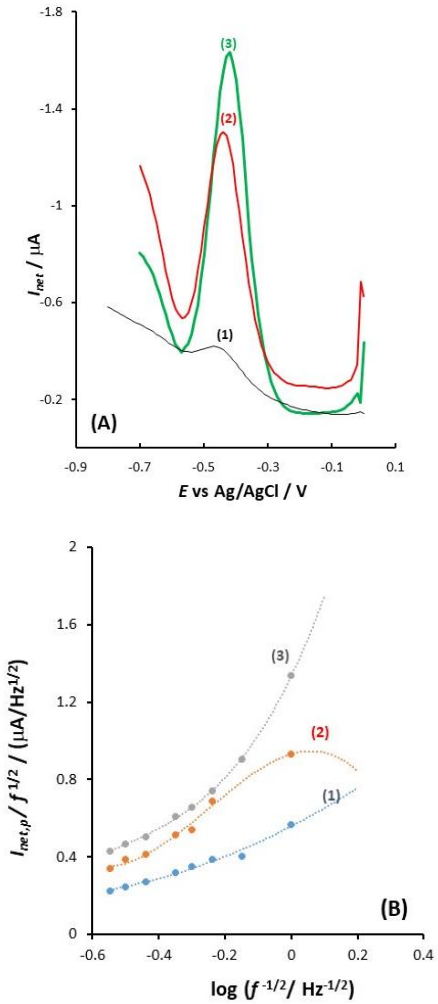

Fig. 6. (A) Typical net SW voltammograms recorded in 0.1 mol/l KOH supporting electrolyte at a bare GC electrode in a degassed solution (1), the Pd@AC modified GC electrode in air-saturated solution (2), and Pd@AC modified GC electrode in the presence of 1 mmol/l H_2O_2 in air-saturated solution (3). The parameters of the potential modulation are SW frequency f = 1 Hz, SW amplitude E_{sw} = 25 mV, and step potential dE = 10 mV. **(B)** The dependence of the frequency-normalized net peak-current on the logarithm of the inverse square root of the SW frequency in 0.1 mol/l KOH supporting electrolyte containing 5 mmol/l H_2O_2 at bare GC electrode in a degassed solution (1), the Pd@AC modified GC electrode in a degassed solution (2), and Pd@AC modified GC electrode in air-saturated solution (3). The other conditions are as in the panel A.

In accordance with the previous CV data, the SW voltammetric response chiefly originates from the electrode reduction of oxygen (curve 2 in Fig. 6A), while the strongest electrocatalytic effect is observed in the presence of both hydrogen peroxide and oxygen (curve 3 in Fig. 6A). The analysis of the SW voltammograms as a function of the SW frequency is presented in Fig. 6B as the dependence of the frequency normalized net peak-current ($I_{net,p}/f^{1/2}$) as a function of the logarithm of the inverse frequency $\log(f^{-1/2})$. Note that the parameter $I_{net,p}/f^{1/2}$ corresponds to the dimensionless current function, reflecting the intrinsic features of the ongoing electrode mechanism.[39] However, the parameter $f^{-1/2}$ corresponds either to the electrode kinetic parameter, reflecting the rate of electron transfer[40], or to the chemical kinetic parameter in the case of $C_{het}E$ mechanism[39], which reflects the rate of the preceding chemical reaction (i.e., Eq. 5).

The increasing part of all curves in Fig. 6B signifies the overall electrode kinetics of the complex irreversible reduction process of oxygen, which is the highest in the presence of hydrogen peroxide in an air-saturated solution (curve 3 in Fig. 6B), agreeing with all previous conclusions. Importantly, the frequency analysis in a degassed solution (curve 2 in Fig. 6B) implies a parabolic variation of the net peak-current with the frequency, in agreement with the recent theoretical prediction for a $C_{het}E$ mechanism[39], where the preceding chemical reaction C_{het} (i.e., the disproportionation of hydrogen peroxide) proceeds as a heterogeneous process on the electrode surface. These data support the general assumption that the overall electrode mechanism in the presence of hydrogen peroxide at the Pd@AC modified GC electrode proceeds according to the CE scheme, where C is the disproportionation of hydrogen peroxide (either or both in the bulk of the solution or/and at the surface of palladium particles), and E is the irreversible electrode reduction of oxygen.

4. CONCLUSIONS

A palladium-amorphous carbon composite (Pd@AC) can be successfully synthesized using a simple hydrothermal method. It can then be employed as an electrocatalyst for the reduction of hydrogen peroxide. In this composite, Pd particles are relatively homogeneously distributed on the carbon substrate. Most Pd particles are likely located within the matrix and covered by a carbon layer. The crystalline structure of the Pd@AC

composite was determined using the XRD method, which confirmed the presence of peaks corresponding to Pd particles and the amorphous nature of the carbon substrate.

The Pd@AC composite exhibits a significant electrocatalytic effect on the electrochemical reduction of H_2O_2 compared to the bare glassy carbon electrode, especially in alkaline conditions. This effect follows a complex reaction pathway described by the CE scheme, where the H_2O_2 disproportionation reaction (C) occurs in both the bulk of the solution and on the Pd particles, and the electrode oxygen reduction (*E*) takes place on the Pd particles.

Acknowledgments. The authors would like to acknowledge financial support from the Ministry of Education, Science and Technological Development of the Republic of Serbia (Agreement No 451-03-68/2020-14/200124). VM acknowledges with gratitude the support from the National Science Center, Poland, through grant No. 2020/39/I/ST4/01854. For the purpose of Open Access, the author has applied a CC-BY public copyright license to any Author Accepted Manuscript (AAM) version arising from this submission.

REFERENCES

(1) Chen W.; Cai S.; Ren Q-Q.; Wen W.; Zhao Y-D, Recent advances in electrochemical sensing for hydrogen peroxide: A review. *Analyst.* **2012**, *137*, 49–58. DOI: https://doi.org/10.1039/C1AN15738H

(2) Butwong N.; Zhou L.; Ng-eontae W.; Burakham R.; Moore E.; Srijaranai S.; Loung J. H. T.; Glennon J. D, A sensitive nonenzymatic hydrogen peroxide sensor using cadmium oxide nanoparticles/multiwall carbon nanotube modified glassy carbon electrode. *J. Electroanal. Chem*. **2014**, *717–718*, 41–46. DOI: http://dx.doi.org/10.1016/j.jelechem.2013.12.028

(3) Klassen N. V.; Marchngton D.; McGowan H. C. E., H_2O_2 determination by the I3-method and by $KMnO_4$ titration. *Anal. Chem.* **1994**, *66*, 2921–2925. DOI: https://doi.org/10.1021/ac00090a020

(4) Steinberg S. M., High-performance liquid chromatography method for determination of hydrogen peroxide in aqueous solution and application to simulated Martian soil and related materials. *Environ. Monit. Assess*. **2013**, *185*, 3749–3757. DOI: 10.1007/s10661-012-2825-4

(5) Hsu C. C.; Lo Y-R.; Lin Y. C.; Shi Y. C.; Li P. L., A spectrometric method for hydrogen peroxide concentration measurement with a reusable and cost-efficient sensor. *Sensors.* **2015**, *15*, 25716–25729. DOI: https://doi.org/10.3390/s151025716

(6) Kosman J.; Juskowiak B., Peroxidase-mimicking DNAzymes for biosensing applications: A review. *Anal. Chim. Acta*. **2011**, *707*, 7–17. DOI: https://doi.org/10.1016/j.aca.2011.08.050

(7) Vdovenko M. M.; Demiyanova A. S.; Kopylov K. E.; Sakharov I. Y., FeIII-TAML activator: a potent peroxidase mimic for chemiluminescent determination of hydrogen peroxide. *Talanta.* **2014**, *125*, 361–365. DOI: http://dx.doi.org/10.1016/j.talanta.2014.03.040

(8) Chandra S.; Lokesh K. S.; Nicolai A.; Lang H., Dendrimer-rhodium nanoparticle modified glassy carbon electrode for amperometric detection of hydrogen peroxide. *Anal. Chim. Acta* **2009**, *632*, 63–68. DOI: https://doi.org/10.1016/j.aca.2008.10.062

(9) Liu M.; Zhao G.; Zhao K.; Tong X.; Tang Y., Direct electrochemistry of hemoglobin at vertically-aligned self-doping TiO_2 nanotubes: A mediator-free and biomolecule-substantive electrochemical interface. *Electrochem. Commun.* **2009**, *11*, 1397–1400. DOI: https://doi.org/10.1016/j.elecom.2009.05.015

(10) Liu M.; Liu R.; Chen W., Graphene wrapped Cu_2O nanocubes: Non-enzymatic electrochemical sensors for the detection of glucose and hydrogen peroxide with enhanced stability. *Biosens. Bioelectron*. **2013**, *45*, 206–212. DOI: https://doi.org/10.1016/j.bios.2013.02.010

(11) Zhang R.; Chen W., Fe_3C-functionalized 3D nitrogen-doped carbon structures for electrochemical detection of hydrogen peroxide. *Sci. Bull*. **2015**, *60*, 522–531. DOI: https://doi.org/10.1007/s11434-015-0740-0

(12) Zhu X.; Yuri I.; Gan X.; Suzuki I.; Li G., Electrochemical study of the effect of nano-zinc oxide on microperoxidase and its application to more sensitive hydrogen peroxide biosensor preparation. *Biosen. Bioelectron*. **2007**, *22*, 1600–1604. DOI: https://doi.org/10.1016/j.bios.2006.07.007

(13) Rashed Md. A.; Ahmed J.; Faisal M.; Alsareii S. A.; Jalalah M.; Tirth V.; Harraz F. A., Surface modification of CuO nanoparticles with conducting polythiophene as a non-enzymatic amperometric sensor for sensitive and selective determination of hydrogen peroxide. *Surf. Interfaces.* **2022**, *31*, 101998. DOI: https://doi.org/10.1016/j.surfin.2022.101998

(14) Kong D-R.; Xin Y-Y.; Li B.; Zhang X-F.; Deng Z-P.; Huo L-H.; Gao S., Non-enzymatic $CuCr_2O_4$/GCE amperometric sensor for high sensing and rapid detection of nM level H_2O_2. *Microchem. J.* **2023,** *194*, 109343. DOI: https://doi.org/10.1016/j.microc.2023.109343

(15) Huang Z-N.; Liu G-C.; Zou J.; Jiang X-Y., Liu Y-P.; Yu J-G., A hybrid composite of recycled popcorn-shaped MnO_2 microsphere and Ox-MWCNTs as a sensitive non-enzymatic amperometric H_2O_2 sensor. *Microchem. J.* **2020**, *158*, 105215. DOI: https://doi.org/10.1016/j.microc.2020.105215

(16) Stradiotto R. N.; Yamanaka H.; Zanoni B. M. V. Electrochemical sensors: a powerful tool in analytical chemistry. *J. Braz. Chem. Soc.* **2003**, *14*. DOI: https://doi.org/10.1590/S0103-50532003000200003

(17) Lorestani F.; Shahnavaz Z.; Mn P.; Alias Y.; Manan N. S. A., Synthesis of silver nanoparticle-carbon nanotube reduced-graphene oxide composite and its application as hydrogen peroxide sensor. *Sens. Actuators B: Chem*. **2015**, *208*, 389–398. DOI: https://doi.org/10.1016/j.snb.2014.11.074

(18) Nazarpour S.; Hajian R.; Sabzvari M. H., A novel nanocomposite electrochemical sensor based on green synthesis of reduced graphene oxide/gold nanoparticles modified screen printed electrode for determination of tryptophan using response surface methodology approach. *Microchem. J*. **2020**, *154*, 104634. DOI: https://doi.org/10.1016/j.microc.2020.104634

(19) Fernandes V. Q.; Silva M. K. L.; Cesarino I., Determination of isotretinoin (13-cis-retinoic acid) using a sensor based on reduced graphene oxide modified with copper nanoparticles. *J. Electroanal. Chem*. **2020**, *856*, 113692. DOI: https://doi.org/10.1016/j.jelechem.2019.113692

(20) Guler M.; Turkoglu V.; Kivrak A.; Karahan F., A novel nonenzymatic hydrogen peroxide amperometric sensor based on Pd@CeO_2-NH_2 nanocomposites modified glassy carbon electrode. *Mater. Sci. Eng. C*. **2018**, *90*, 454–460. DOI: https://doi.org/10.1016/j.msec.2018.04.084

(21) Yi W.; Li Z.; Dong C.; Li H-W.; Li J., Electrochemical detection of chloramphenicol using palladium nanoparticles decorated reduced graphene oxide. *Microchem. J.* **2019**, *148*, 774–783. DOI: https://doi.org/10.1016/j.microc.2019.05.049

(22) Zheng J-N.; Li S-S.; Ma X.; Chen F-Y.; Wang A-J.; Chen J-R.; Feng J-J., Green synthesis of core–shell gold–palladium@palladium nanocrystals dispersed on graphene with enhanced catalytic activity toward oxygen reduction and methanol oxidation in alkaline media. *J. Power Sources*. **2014**, *262*, 270–278. DOI: https://doi.org/10.1016/j.jpowsour.2014.03.131

(23) Venkatachalapathy R.; Davila P. G.; Prakash J., Catalytic decomposition of hydrogen peroxide in alkaline solutions. *Electrochem. Commun.* **1999**, *1*, 614–617. DOI: https://doi.org/10.1016/S1388-2481(99)00126-5

(24) Hall B. S.; Khudaish A. E.; Hart L. A., Electrochemical oxidation of hydrogen peroxide at platinum electrodes. Part 1. An adsorption-controlled mechanism. *Electrochim. Acta*, **1998**, *43*, 579–588. DOI: https://doi.org/10.1016/S0013-4686(97)00125-4

(25) Shao M.; Yu T.; Odell J. H.; Jin M.; Xia Y., Structural dependence of oxygen reduction reaction on palladium nanocrystals. *Chem. Commun*. **2011**, *47*, 6566–6568. DOI: https://doi.org/10.1039/C1CC11004G

(26) Sokolov S. V.; Sepunaru L.; Compton R. G., Taking cues from nature: Hemoglobin catalysed oxygen reduction. *Appl. Mater. Today*. **2017**, *7*, 82–90. DOI: https://doi.org/10.1016/j.apmt.2017.01.005

(27) Čović J.; Mirceski V.; Zarubica A.; Enke D.; Carstens S.; Bojić A.; Ranđelović M., Palladium-graphene hybrid as an electrocatalyst for hydrogen peroxide reduction. *Appl. Surf. Sci*. **2022**, *574*, 151633. DOI: https://doi.org/10.1016/j.apsusc.2021.151633

(28) Elsheikh A.; Martins V. L.; McGregor J., Influence of physiochemical characteristics of carbon supports on Pd ethanol oxidation catalysts. *Energy Procedia* **2018**, *151*, 79–83. DOI: https://doi.org/10.1016/j.egypro.2018.09.031

(29) Chen S.; Wang G.; Sui W.; Parvez A. M.; Dai L.; Si C., Novel lignin-based phenolic nanosphere supported palladium nanoparticles with highly efficient catalytic performance and good reusability. *Ind. Crops Prod*. **2020**, *145*, 112164. DOI: https://doi.org/10.1016/j.indcrop.2020.112164

(30) Wei Z.; Yan P.; Feng W.; Dai J.; Wang Q.; Xia T., Monostructural characterization of Ni nanoparticles prepared by anodic arc plasma. *Mater. Charact*. **2006**, *57*, 176–181. DOI: https://doi.org/10.1016/j.matchar.2006.01.004

(31) Ng J. C.; Tan C. Y.; Ong B. H.; Matsuda A.; Basirun W. J.; Tan W. K.; Singh R.; Yap B. K., Novel palladium-guanine-reduced graphene oxide nanocomposite as efficient electrocatalyst for methanol oxidation reaction. *Mater. Res. Bull*. **2019**, *112*, 213–220. DOI: https://doi.org/10.1016/j.materresbull.2018.12.029

(32) Poljanšek I.; Krajnc M., Characterization of phenol-formaldehyde prepolymer resins by in line FT-IR spectroscopy. *Acta Chim. Slov.* **2005**, *52*, 238–244.

(33) Yangfei C.; Zhiqin C.; Shaoyi X.; Hongbo L., A novel thermal degradation mechanism of phenol–formaldehyde type resins. *Thermochim. Acta*. **2008**, *476*, 39–43. DOI: https://doi.org/10.1016/j.tca.2008.04.013

(34) Calvo E. J.; Schiffrin D. J., The reduction of hydrogen peroxide on passive iron in alkaline solutions. *J. Electroanal. Chem.* **1984**, *163*, 257–275. DOI: https://doi.org/10.1016/S0022-0728(84)80056-X

(35) Nagaiah T.C.; Schäfer D.; Schuhmann W.; Dimcheva N. Electrochemically deposited Pd−Pt and Pd−Au codeposits on graphite electrodes for electrocatalytic H_2O_2 reduction. *Anal. Chem*. **2013**, *85*, 7897–7903. DOI: https://doi.org/10.1021/ac401317y

(36) Marceta Kaninski M .P.; Saponjic Dj. P.; Perovic I. M.; Maksic A. D.; Nikolic V. M., Electrochemical characterization of the Ni–W catalyst formed in situ during alkaline electrolytic hydrogen production. Part II. *Appl. Catal. A: Gen*. **2011**, *405*, 29–35. DOI: https://doi.org/10.1016/j.apcata.2011.07.015

(37) Scholz F., *Electroanalytical Methods*. Guide to Experiments and Applications. Second, revised and extended edition. Springer, Heidelberg–Dordrecht London–New York, 2010. DOI: https://doi.org/10.1007/978-3-642-02915-8

(38) Poux T.; Bonnefont A.; Ryabova A.; Kéranguéven G.; Tsirlina G. A.; Savinova E. R., Electrocatalysis of hydrogen peroxide reactions on perovskite oxides: experiment versus kinetic modeling. *Physical Chemistry Chemical Physics*. **2014**, *16*, 13595–13600. DOI: https://doi.org/10.1039/C4CP00341A

(39) Mirceski V.; Gulaboski R.; Compton G. R. Distinguishing heterogeneous and homogeneous CE mechanisms: theoretical insights in square-wave voltammetry. *J. Phys. Chem. C*. **2023**, *127*, 3437−3443. DOI: https://doi.org/10.1021/acs.jpcc.2c07298

(40) Mirceski V.; Skrzypek S.; Stojanov L., Square-wave voltammetry. *Chem Texts*. **2018**, *4*, 17–3. DOI: 10.1007/s40828-018-0073-0